nature physics

ARTICLES

PUBLISHED ONLINE: 23 MARCH 2014 | DOI: 10.1038/NPHYS2911

Bidirectional and efficient conversion between microwave and optical light

R. W. Andrews[1,2*], R. W. Peterson[1,2], T. P. Purdy[1,2], K. Cicak[3], R. W. Simmonds[3], C. A. Regal[1,2] and K. W. Lehnert[1,2,3]

Converting low-frequency electrical signals into much higher-frequency optical signals has enabled modern communication networks to leverage the strengths of both microfabricated electrical circuits and optical fibre transmission, enabling information networks to grow in size and complexity. A microwave-to-optical converter in a quantum information network could provide similar gains by linking quantum processors through low-loss optical fibres and enabling a large-scale quantum network. However, no current technology can convert low-frequency microwave signals into high-frequency optical signals while preserving their fragile quantum state. Here we demonstrate a converter that provides a bidirectional, coherent and efficient link between the microwave and optical portions of the electromagnetic spectrum. We use our converter to transfer classical signals between microwave and optical light with conversion efficiencies of ∼10%, and achieve performance sufficient to transfer quantum states if the device were further precooled from its current 4 K operating temperature to temperatures below 40 mK.

Modern communication networks manipulate information at several gigahertz with microprocessors and distribute information at hundreds of terahertz through optical fibres. A similar frequency dichotomy is developing in quantum information processing. Superconducting qubits operating at several gigahertz have recently emerged as promising high-fidelity and intrinsically scalable quantum processors[1–3]. Conversely, optical frequencies provide access to low-loss transmission[4] and long-lived quantum-compatible storage[5,6]. Converting information between gigahertz-frequency 'microwave light' that can be deftly manipulated and terahertz-frequency 'optical light' that can be efficiently distributed will enable small-scale quantum systems[7–9] to be combined into larger, fully functional quantum networks[10,11]. However, no current technology can transform information between these vastly different frequencies while preserving the fragile quantum state of the information. For this demanding application, a frequency converter must provide a near-unitary transformation between microwave light and optical light; that is, the ideal transformation is coherent, lossless and noiseless.

Certain nonlinear materials provide a link between microwave and optical light, and these are commonly used in electro-optic modulators for just this purpose. Although electro-optic modulators might be capable of quantum-compatible frequency conversion[12,13], such conversion has not yet been demonstrated, and current electro-optic modulators[14–16] have predicted photon number efficiencies of only a few 10^{-4} (refs 12,13,15). Other intermediate objects that interact with both microwave and optical light can be used to create the nonlinearity necessary for frequency conversion. Proposed intermediaries include clouds of ultracold atoms[17,18], ensembles of spins[19,20] and mechanical resonators[21–23]. All converters face the challenge of integrating optical light with the cryogenic temperatures needed for low-noise microwave signals and superconducting circuitry. Here, we demonstrate a cryogenic converter that incorporates a mechanical resonator with optical light and superconducting circuitry, and use it to transform classical signals between microwave and optical frequencies.

Early experiments used microwave light[24,25] and optical light[26] to manipulate mechanical resonators and study the interaction between light and a vibrating mass[27,28]. The fields of electromechanics and optomechanics have since evolved at a remarkably commensurate pace. Both microwave and optical light have been separately used to cool a mechanical resonator to its quantum ground state of motion[29,30]. This same interaction enables the mechanical resonator to serve as an information storage medium[31,32], and opens up the possibility of high-fidelity frequency conversion[33–37]. By combining the technologies of electromechanics and optomechanics, we simultaneously couple a mechanical resonator to both a microwave circuit and an optical cavity. This simultaneous coupling enables information in the microwave domain to stream through the mechanical resonator and emerge as optical light, and vice versa. We show that the transformation is bidirectional and coherent, and further demonstrate a photon number efficiency of 0.086 ± 0.007 and a transfer bandwidth of 30 kHz. Furthermore, the performance is sufficient for nearly noiseless frequency conversion if we can further precool the device from its current 4 K operating temperature to dilution refrigerator temperatures below 40 mK.

Cavity electro-optomechanics

Our converter consists of two electromagnetic resonators, one at an optical frequency and one at a microwave frequency, that share a mechanical resonator. The mechanical resonator is formed by a thin silicon nitride membrane that is free to vibrate (Fig. 1). The optical frequency resonator consists of a Fabry–Pérot cavity, and as the membrane vibrates it moves along the optical intensity standing wave and modulates the resonant frequency of the optical cavity[38,39]. The membrane is partially coated with a thin layer of niobium (which superconducts at temperatures below

[1]JILA, University of Colorado and NIST, Boulder, Colorado 80309, USA, [2]Department of Physics, University of Colorado, Boulder, Colorado 80309, USA, [3]National Institute of Standards and Technology (NIST), Boulder, Colorado 80305, USA. *e-mail: reed.andrews@colorado.edu

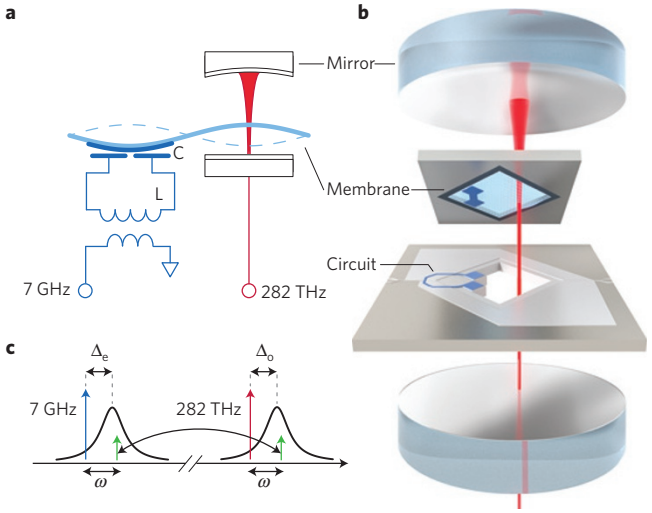

Figure 1 | Layout and operation of microwave-to-optical converter. a, A stoichiometric silicon nitride (Si_3N_4) membrane (light blue) that has been partially covered with niobium (dark blue) interacts with an inductor–capacitor (LC) circuit that forms the microwave resonator and a Fabry–Pérot cavity that forms the optical resonator (mode shown in red). Propagating light fields are coupled to the microwave resonator with an inductive coupler, and to the optical resonator with a slightly transmissive input mirror. **b**, The membrane is suspended within a silicon frame, and the microwave circuitry is lithographically patterned on a separate silicon substrate. The two silicon chips are brought together so that the niobium-covered portion of the membrane comes to within 500 nm of the microwave circuitry, thus forming the electromechanical system. The system is then placed inside the optical resonator. The entire structure is designed to be cryogenically compatible. **c**, A frequency domain representation of the conversion process. A strong microwave pump (blue arrow) is applied below the microwave resonance (response shown as a black curve) with detuning Δ_e. Likewise, a strong optical pump (red arrow) is applied below the optical resonance (response shown as a black curve) with detuning Δ_o. This enables a signal (green arrow) to be up- or down-converted in frequency.

about 9 K), and this electrically conductive portion is part of a capacitor in an inductor–capacitor circuit that forms the microwave resonator (K.C., in preparation)[40,41]. As the membrane vibrates, it modulates the capacitance of the microwave circuit, and thus its resonant frequency. Even though the electromagnetic resonators are at vastly different frequencies (7 GHz and 282 THz), the coupling mechanism is equivalent: a nanometre of membrane motion shifts the microwave resonant frequency by approximately 4 MHz, and shifts the optical resonant frequency by approximately 40 MHz, giving coupling constants of $G_e \approx 4\,\mathrm{MHz\,nm^{-1}}$ and $G_o \approx 40\,\mathrm{MHz\,nm^{-1}}$.

During the experiment, a strong pump tone is applied below the resonant frequency of each electromagnetic resonator. The pumps enhance the electromechanical and optomechanical interaction, and the mechanical resonator exchanges information with the microwave and optical resonators at rates $g_e = G_e x_{zp}\sqrt{n_e}$ and $g_o = G_o x_{zp}\sqrt{n_o}$, respectively, where x_{zp} is the zero-point motion of the mechanical resonator and n_e (n_o) is the number of photons in the microwave (optical) resonator induced by the microwave (optical) pump. The expressions for g_e and g_o take on this simple form in the resolved-sideband limit (defined as $4\omega_m \gg \kappa_e, \kappa_o$, where ω_m is the frequency of the vibrational mode of the mechanical resonator and κ_e and κ_o are the energy decay rates of the microwave and optical resonators, respectively); however, these coupling rates can always be independently adjusted *in situ* by changing the strength of the pumps and altering n_e and n_o (ref. 32). This coherent exchange of information between electromagnetic and vibrational modes is capable of quantum-state-preserving frequency conversion[42,43].

A full description of the system includes the inputs and outputs of the microwave, optical and mechanical resonators. Of all the energy leaving the microwave (optical) resonator, only a fraction η_e (η_o) exits into the propagating mode that we collect. Some energy is absorbed in the resonators themselves, and the optical resonator emits light into a particular spatial mode that does not perfectly match the spatial mode of the incident light field. The fraction of light we collect can be expressed as $\eta_e = \kappa_{e,ext}/\kappa_e$ and $\eta_o = \epsilon\kappa_{o,ext}/\kappa_o$, where $\kappa_{e,ext}$ ($\kappa_{o,ext}$) is the rate at which energy leaves the microwave (optical) resonator into propagating fields, and ϵ is the optical mode matching. If $\kappa_e \gg g_e$ and $\kappa_o \gg g_o$, the electromagnetic resonators couple energy and information in freely propagating microwave (optical) modes to a vibrational mode of the mechanical resonator at a rate Γ_e (Γ_o), which has the simple form $\Gamma_e = 4g_e^2/\kappa_e$ ($\Gamma_o = 4g_o^2/\kappa_o$) in the resolved-sideband limit[44].

During upconversion, an injected microwave field enters the converter at a frequency ω above the microwave pump, enters and exits the mechanical resonator as determined by coupling rates Γ_e and Γ_o, and emerges as an outgoing optical field at a frequency ω above the optical pump. A frequency-domain representation of the process is shown in Fig. 1c. Converter performance is characterized by how efficiently the input microwave field, $b_{in}(\omega)$, is transformed into an output optical field, $a_{out}(\omega)$, and vice versa. The ratio $a_{out}(\omega)/b_{in}(\omega) \equiv t_1(\omega)$ is one of four transmission/reflection coefficients that characterize the two-port network formed by the converter (Fig. 2a). The fields $b_{in}(\omega)$ and $a_{out}(\omega)$ have units of $(\mathrm{number} \times \mathrm{sec})^{1/2}$, and so the apparent photon number efficiency for upconversion is given by $|a_{out}(\omega)/b_{in}(\omega)|^2 = |t_1(\omega)|^2$.

During the experiment, the converter is integrated into a larger network. To predict and measure converter performance, we need to specify which components are part of the converter, and which are part of the measurement network. We choose to define the converter as all the components between the inductive coupler of the microwave resonator and the input mirror of the optical resonator (Fig. 2). Converter performance then includes internal losses in the microwave, optical and mechanical resonators and imperfect optical mode matching, but excludes losses and gains in other components that are used in our measurement. With this definition, the converter is a stand-alone component that can be readily integrated into other networks. We can predict converter efficiency using a Hamiltonian that includes radiation pressure coupling[45] to generate Heisenberg–Langevin equations of motion (Supplementary Information). This analysis predicts

$$t_1(\omega) = \frac{\sqrt{\Gamma_e\Gamma_o}}{-\imath\,(\omega-\omega_m)+(\Gamma_e+\Gamma_o+\kappa_m)/2} \times \sqrt{\mathcal{A}\eta_e\eta_o} \qquad (1)$$

where κ_m is the intrinsic mechanical damping and $\mathcal{A} = \mathcal{A}_e\mathcal{A}_o$ is the conversion gain, with $\mathcal{A}_e = 1 + (\kappa_e/4\omega_m)^2$ and $\mathcal{A}_o = 1 + (\kappa_o/4\omega_m)^2$. The reverse process, $t_2(\omega)$, is mathematically identical (Fig. 2a). The bandwidth of the conversion is set by the total mechanical damping $\Gamma_e + \Gamma_o + \kappa_m$. Conversion efficiency is greatest on mechanical resonance ($\omega = \omega_m$) and when the coupling rates are matched ($\Gamma_e = \Gamma_o$) and exceed any intrinsic mechanical damping κ_m; in this case, the maximum conversion efficiency is $\eta_e\eta_o$.

Conversion gain $\mathcal{A}$ becomes appreciable when $4\omega_m < \kappa_e, \kappa_o$ (and also depends on detunings Δ_e and Δ_o; Supplementary Information). In this parameter regime, the converter begins to act like a linear, phase-insensitive amplifier, and as such can have an apparent efficiency greater than unity at the cost of adding noise[46]. Although amplification might be beneficial for some applications, ideal frequency conversion requires unit gain ($\mathcal{A}_e = \mathcal{A}_o = 1$) so that conversion adds as little noise as possible.

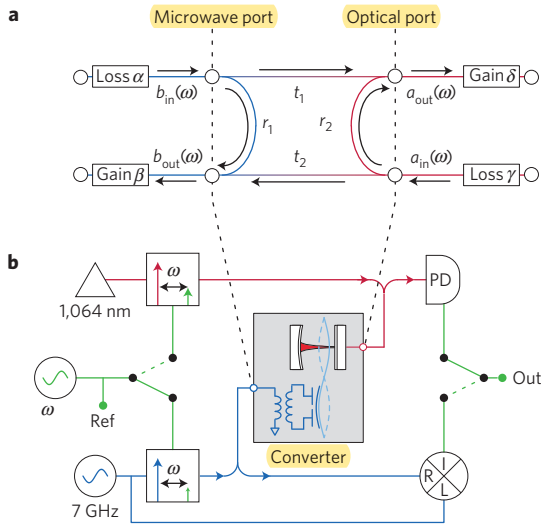

Figure 2 | Measurement network. a, Transmission and reflection coefficients are defined between the ports of the microwave and optical resonators. To isolate the converter performance from the gains and losses of other components used in our measurement, we measure the forward and reverse transmission, $\alpha t_1 \delta$ and $\gamma t_2 \beta$, and the off-resonant reflections, $\alpha\beta$ and $\gamma\delta$. This gives $t_1 t_2 = (\alpha t_1 \delta)(\gamma t_2 \beta)/(\alpha\beta)(\gamma\delta)$, a quantity insensitive to imperfect measurement of the separate gains and losses α, β, γ and δ. The off-resonant reflections are measured by tuning the injected signal away from the resonator's central frequency, where the converter acts as a near-perfect mirror. **b**, A signal at a frequency $\omega \approx \omega_m$ is generated. This signal is mixed to a higher frequency using either the microwave pump or the optical pump as a carrier through single-sideband modulation. After interacting with the converter, the outgoing fields are detected with homodyne detection (for microwave frequencies) or direct detection with a photodiode (for optical frequencies). The detected signal (Out) is compared with the initial signal (Ref) to obtain a magnitude and phase shift.

Bidirectional frequency conversion

By injecting a microwave or optical field and monitoring the outgoing fields, we measure the transmission coefficients t_1 and t_2 that give the number efficiency of the converter (Fig. 2b). We study conversion using three different vibrational modes of the mechanical resonator, which are shown as membrane-displacement plots in Fig. 3a. Converter performance using the $\omega_m/2\pi = 560$ kHz vibrational mode is shown in Fig. 3c. By sweeping the frequency of the injected microwave signal, we confirm that forward transmission (t_1) has the expected Lorentzian lineshape of equation (1), with a peak at $\omega = \omega_m$. Reverse transmission (t_2) is the same to within our measurement error, giving an initial indication that the conversion process is bidirectional. We also monitor microwave reflection (r_1) during upconversion. When conversion efficiency peaks at $\omega = \omega_m$, there is a corresponding dip in reflected microwave power, as seen in Fig. 3c, further demonstrating that some of the injected microwave signal is indeed being converted. In addition to the magnitudes of the converted and reflected light, the measurements also yield phase information. We find that, up to a frequency-dependent phase shift, the phase is preserved during conversion, indicating that the conversion between the two frequency regimes is coherent.

Although it is difficult to independently and accurately calibrate the quantities t_1 and t_2, we can readily calibrate their product, as diagrammed in Fig. 2a. With this method, we can determine $t_1 t_2$ to about 6% (limited by a combination of standing waves in the microwave transmission lines and loss of optical phase information during direct photodetection; Supplementary Information). We find this calibration procedure appealing because it makes equivalent use of both the forward and reverse transmission of the converter, demonstrating and emphasizing its bidirectional nature. The peak value of the apparent conversion efficiency, plotted as $|t_1 t_2|$, is shown in Fig. 3b along with the microwave reflection, $|r_1|^2$, at the frequency of peak conversion efficiency.

The converter performance for all three vibrational modes is correctly predicted by linear optomechanical theory with independently measured system parameters (Supplementary Information). By changing the microwave pump power while holding the optical pump power fixed, we vary the ratio Γ_e/Γ_o and observe that maximum conversion efficiency occurs near $\Gamma_e = \Gamma_o$, as seen in Fig. 3b, confirming the impedance matching condition predicted by equation (1). Furthermore, we can explore the effect of conversion gain by using different vibrational modes of the mechanical resonator for frequency conversion. For the $\omega_m/2\pi = 380$ kHz vibrational mode, $\omega_m/\kappa_e \approx \omega_m/\kappa_o \approx 0.25$ and a photon number gain of $\mathcal{A} = 3$ is expected. This results in an apparent efficiency of 0.25, as seen in the peak value of $|t_1 t_2|$ for this vibrational mode. For conversion with the higher-frequency $\omega_m/2\pi = 1.24$ MHz vibrational mode, $\omega_m/\kappa_e \approx \omega_m/\kappa_o \approx 0.8$ and the converter approaches the resolved-sideband limit. This reduces the photon number gain to $\mathcal{A} = 1.4$. With this lower gain comes a lower apparent efficiency, but the absorption of microwave power occurs nearer the peak in conversion efficiency, indicating more ideal conversion (Supplementary Information).

The converter reaches nearly unit internal efficiency for $\Gamma_e, \Gamma_o \gg \kappa_m$. For the $\omega_m/2\pi = 560$ kHz vibrational mode, the converter reaches a matched ($\Gamma_e = \Gamma_o$) bandwidth of 30 kHz, overwhelming the intrinsic mechanical loss by nearly four orders of magnitude; that is, only about two parts in 10^4 of the converted signal are lost through the mechanical decay channel. For this vibrational mode, we expect the maximum *apparent* conversion efficiency to be $|t_1 t_2| = \mathcal{A}\eta_e\eta_o = 0.169 \pm 0.012$, which corresponds well to the measured maximum of 0.178 ± 0.011. The true efficiency $\eta_e\eta_o$, which does not include conversion gain $\mathcal{A}$, is limited by absorption and scattering of light in the electromagnetic resonators ($\kappa_{e,ext}/\kappa_e = 0.76$ and $\kappa_{o,ext}/\kappa_o = 0.23$), and imperfect optical mode matching ($\epsilon = 0.47$). These factors combine to give an expected efficiency $\eta_e\eta_o = 0.082 \pm 0.006$. This corresponds well with the measured maximum apparent efficiency divided by the expected gain of 0.086 ± 0.007.

Vibrational noise

Any extraneous vibrations of the mechanical resonator appear as noise on the converted signal, and can be specified with a signal-to-noise ratio, defined as $\mathrm{SNR} = \mathcal{S}_{in}/n_{vib}$, where $\mathcal{S}_{in}$ is the spectral density of the input signal, and n_{vib} is the spectral density of vibrational noise added during conversion as referenced to the input of the converter[44]. In units of quanta of added noise (a quantum corresponding to one photon per second in a 1 Hz bandwidth), upconversion adds

$$n_{vib} = \frac{1}{\mathcal{A}_e\eta_e}\left(\frac{\kappa_m n_{env}}{\Gamma_e} + (\mathcal{A}_e - 1) + (\mathcal{A}_o - 1)\right) \qquad (2)$$

for matched coupling rates, where $n_{env} \equiv 1/(e^{\hbar\omega_m/k_B T_{env}} - 1)$, k_B is Boltzmann's constant and T_{env} is the temperature of the mechanical resonator's environment. Any conversion gain adds vibrational noise given by the last two terms in equation (2). Mechanical decoherence $\kappa_m n_{env}$ also adds vibrational noise, but the effect of mechanical decoherence can be reduced by increasing Γ_e and Γ_o. Only with unit gain ($\eta_e \gg \mathcal{A}_e - 1$ and $\eta_e \gg \mathcal{A}_o - 1$) and negligible mechanical decoherence ($\eta_e\Gamma_e \gg \kappa_m n_{env}$) do vibrations of the mechanical resonator 'freeze out'. In addition to low vibrational noise, noiseless frequency conversion requires unit conversion efficiency ($\eta_e = \eta_o = 1$).

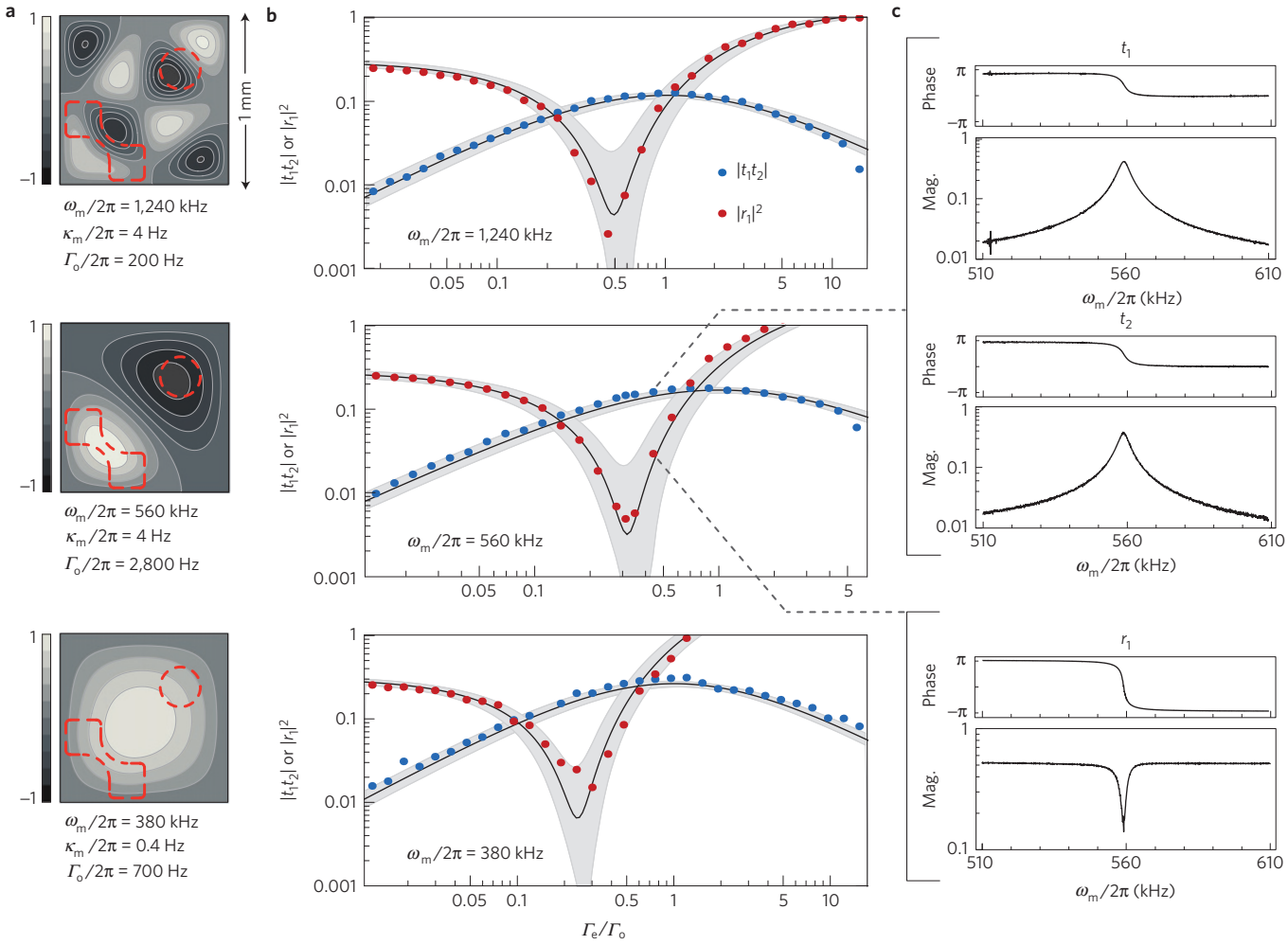

Figure 3 | Bidirectional and efficient conversion. a, Contour plot of simulated membrane displacement, normalized to unity, for the three vibrational modes used for frequency conversion. Outlines of the optical mode (dashed circle) and niobium metallization (dashed bowtie) are shown. **b**, Apparent transfer efficiency ($|t_1t_2|$), depicted by blue points, and microwave-power reflection coefficient ($|r_1|^2$), depicted by red points, as a function of damping ratio for the three vibrational modes. The measurement error is smaller than the plotted points. The black lines are expected values given independently measured system parameters. Grey regions express the uncertainty of our system parameters (Supplementary Information). **c**, Forward transmission (t_1), reverse transmission (t_2) and microwave reflection (r_1) for the $\omega_m/2\pi = 560$ kHz vibrational mode with $\Gamma_o/2\pi = 2{,}800$ Hz and $\Gamma_e/2\pi = 1{,}300$ Hz. Frequency is relative to the microwave and optical pump frequencies. Electromagnetic resonators are centred at 7.1 GHz and 282 THz, with power decay rates $\kappa_e/2\pi = 1.6$ MHz and $\kappa_o/2\pi = 1.65$ MHz and efficiencies $\eta_e = 0.76$ and $\eta_o = 0.11$ (0.23 from internal resonator loss and 0.47 from optical mode matching). Pumps are red-detuned with $\Delta_e \approx -\omega_m$ and $\Delta_o/2\pi = -730$ kHz (Supplementary Information).

To characterize noise added by vibrations of the mechanical resonator, we inject a fixed-frequency signal into the microwave port of the converter and measure the spectral density of the output optical field. We measure vibrational noise added during upconversion (as opposed to downconversion) because near-quantum-limited photodetection enables us to quickly characterize noise at optical frequencies. The microwave signal is injected at a frequency ω_m above the microwave pump with matched coupling rates ($\Gamma_e \approx \Gamma_o$). As shown in the inset of Fig. 4, the converted signal power appears on a noise background that is dominated by thermal fluctuations filtered by the mechanical resonator's susceptibility. As we increase the coupling rates Γ_e and Γ_o (while keeping the injected microwave signal power constant), we observe an increased signal-to-noise ratio (Fig. 4). Fitting the observed signal-to-noise ratio to linear optomechanical theory for the spectral density of the injected microwave signal S_{in} enables us to estimate n_{vib}, the added vibrational noise.

Vibrational noise is non-zero during 4 K operation because the mechanical resonator is still 'hot' and driven by thermal fluctuations. Although this effect can be substantially reduced by increasing Γ_e and Γ_o, lower temperatures are needed to reduce added vibrational noise to the single-quantum level. Thermalizing the vibrational modes of the mechanical resonator to a dilution refrigerator temperature of 40 mK with the achieved $\Gamma_e = \Gamma_o = 2\pi \times 15$ kHz would ideally result in $n_{vib} \approx 1$. Spurious mechanical modes in the silicon substrate and mirrors that are another potential source of noise are also expected to be suppressed at colder temperatures[47]. Furthermore, temperatures of $T_{env} < (2\pi \times 7\ \text{GHz})\hbar/k_B \approx 300$ mK are required to eliminate Johnson noise at microwave frequencies, which corrupts weak (quantum) signals.

Discussion

We have demonstrated a converter that provides a bidirectional, coherent and efficient link between the microwave and optical portions of the electromagnetic spectrum. Three features we have observed—the bidirectionality of the conversion, its phase-preserving nature and the absorption of injected signal power during conversion—provide firm evidence that state transfer

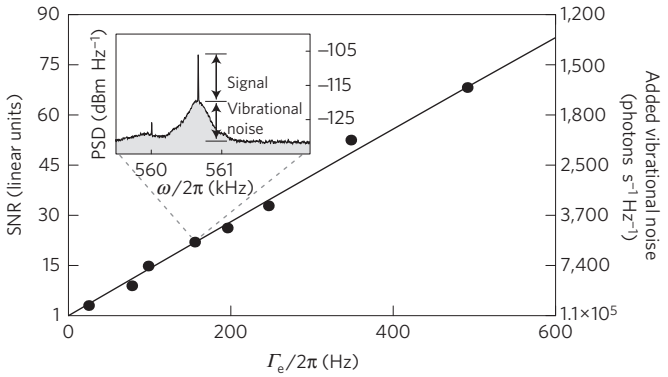

Figure 4 | Optically detected signal-to-noise ratio. Signal-to-noise ratio (SNR) for an upconverted microwave signal as a function of coupling rate Γ_e; injected signal power is kept constant and $\Gamma_o \approx \Gamma_e$. A fit to optomechanical theory is shown (line), and the extracted added vibrational noise (n_{vib}) is shown on the right vertical axis. Inset: power spectral density (PSD) of an upconverted microwave signal.

is occurring, and that we have accessed the beam-splitter Hamiltonian[43] that is fundamentally capable of noiseless state transfer. The ability to coherently exchange information between microwave and optical light opens new possibilities for quantum information, in particular entanglement between microwave and optical photons[36,48–50].

Although the converter functions well, some modest changes can significantly improve performance. Removing internal loss in the electromagnetic resonators will improve η_e and η_o, which currently limit conversion efficiency. Lower temperatures will improve the microwave resonator, which at 4 K suffers from thermally excited quasiparticles that limit η_e. Constructing the optical resonator with asymmetric mirror coatings will improve η_o by reducing the amount of light lost through the second mirror. In addition, more careful placement of the electromechanical system inside the optical resonator can decrease scattered light and improve optical mode matching[39]. Added vibrational noise can be reduced by using mechanical resonators with higher quality factors ($Q \equiv \omega_m/\kappa_m$). In particular, the type of silicon nitride membrane we use is capable of extremely high quality factors of $Q > 10^7$ (refs 40,47,51), about two orders of magnitude greater than the quality factors used in this work. With our modular converter design, improvements to any single converter component can be carried out independently. This inherent flexibility will enable us to explore the materials and methods necessary to fully integrate optical light with superconducting qubits at millikelvin temperatures.

Received 09 October 2013; accepted 07 February 2014; published online 23 March 2014

References

1. Clarke, J. & Wilhelm, F. K. Superconducting quantum bits. *Nature* **453,** 1031–1042 (2008).
2. Schoelkopf, R. J. & Girvin, S. M. Wiring up quantum systems. *Nature* **451,** 664–669 (2008).
3. Devoret, M. H. & Schoelkopf, R. J. Superconducting circuits for quantum information: An outlook. *Science* **339,** 1169–1174 (2013).
4. O'Brien, J. L., Furusawa, A. & Vuckovic, J. Photonic quantum technologies. *Nature Photon.* **3,** 687–695 (2009).
5. Buluta, I., Ashhab, S. & Nori, F. Natural and artificial atoms for quantum computation. *Rep. Prog. Phys.* **74,** 104401 (2011).
6. Langer, C. *et al.* Long-lived qubit memory using atomic ions. *Phys. Rev. Lett.* **95,** 060502 (2005).
7. Ritter, S. *et al.* An elementary quantum network of single atoms in optical cavities. *Nature* **484,** 195–200 (2012).
8. Reed, M. D. *et al.* Realization of three-qubit quantum error correction with superconducting circuits. *Nature* **482,** 382–385 (2012).
9. Lucero, E. *et al.* Computing prime factors with a Josephson phase qubit quantum processor. *Nature Phys.* **8,** 719–723 (2012).
10. Kimble, H. J. The quantum internet. *Nature* **453,** 1023–1030 (2008).
11. Ladd, T. D. *et al.* Quantum computers. *Nature* **464,** 45–53 (2010).
12. Tsang, M. Cavity quantum electro-optics. *Phys. Rev. A* **81,** 063837 (2010).
13. Tsang, M. Cavity quantum electro-optics. II. input–output relations between traveling optical and microwave fields. *Phys. Rev. A* **84,** 043845 (2011).
14. Cohen, D. A., Hossein-Zadeh, M. & Levi, A. F. J. Microphotonic modulator for microwave receiver. *Electron. Lett.* **37,** 300–301 (2001).
15. Ilchenko, V. S., Savchenkov, A. A., Matsko, A. B. & Maleki, L. Whispering-gallery-mode electro-optic modulator and photonic microwave receiver. *J. Opt. Soc. Am. B* **20,** 333–342 (2003).
16. Savchenkov, A. A. *et al.* Tunable optical single-sideband modulator with complete sideband suppression. *Opt. Lett.* **34,** 1300–1302 (2009).
17. Hafezi, M. *et al.* Atomic interface between microwave and optical photons. *Phys. Rev. A* **85,** 020302 (2012).
18. Verdú, J. *et al.* Strong magnetic coupling of an ultracold gas to a superconducting waveguide cavity. *Phys. Rev. Lett.* **103,** 043603 (2009).
19. Imamoğlu, A. Cavity QED based on collective magnetic dipole coupling: Spin ensembles as hybrid two-level systems. *Phys. Rev. Lett.* **102,** 083602 (2009).
20. Marcos, D. *et al.* Coupling nitrogen-vacancy centers in diamond to superconducting flux qubits. *Phys. Rev. Lett.* **105,** 210501 (2010).
21. Safavi-Naeini, A. H. & Painter, O. Proposal for an optomechanical traveling wave phonon-photon translator. *New J. Phys.* **13,** 013017 (2011).
22. Regal, C. A. & Lehnert, K. W. From cavity electromechanics to cavity optomechanics. *J. Phys.: Conf. Ser.* **264,** 012025 (2011).
23. Bochmann, J., Vainsencher, A., Awschalom, D. D. & Cleland, A. N. Nanomechanical coupling between microwave and optical photons. *Nature Phys.* **9,** 712–716 (2013).
24. Braginsky, V., Manukin, A. B. & Tikhonov, M. Y. Investigation of dissipative ponderomotive effects of electromagnetic radiation. *J. Exp. Theor. Phys.* **31,** 829–830 (1970).
25. Gozzini, A., Maccarrone, F., Mango, F., Longo, I. & Barbarino, S. Light-pressure bistability at microwave frequencies. *J. Opt. Soc. Am. B* **2,** 1841–1845 (1985).
26. Dorsel, A., McCullen, J. D., Meystre, P., Vignes, E. & Walther, H. Optical bistability and mirror confinement induced by radiation pressure. *Phys. Rev. Lett.* **51,** 1550–1553 (1983).
27. Braginsky, V. & Manukin, A. B. Ponderomotive effects of electromagnetic radiation. *J. Exp. Theor. Phys.* **25,** 563–655 (1967).
28. Caves, C. M. Quantum-mechanical radiation-pressure fluctuations in an interferometer. *Phys. Rev. Lett.* **45,** 75–79 (1980).
29. Teufel, J. D. *et al.* Sideband cooling of micromechanical motion to the quantum ground state. *Nature* **475,** 359–363 (2011).
30. Chan, J. *et al.* Laser cooling of a nanomechanical oscillator into its quantum ground state. *Nature* **478,** 89–92 (2011).
31. Verhagen, E., Deleglise, S., Weis, S., Schliesser, A. & Kippenberg, T. J. Quantum-coherent coupling of a mechanical oscillator to an optical cavity mode. *Nature* **482,** 63–67 (2012).
32. Palomaki, T. A., Harlow, J. W., Teufel, J. D., Simmonds, R. W. & Lehnert, K. W. Coherent state transfer between itinerant microwave fields and a mechanical oscillator. *Nature* **495,** 210–214 (2013).
33. Tian, L. & Wang, H. Optical wavelength conversion of quantum states with optomechanics. *Phys. Rev. A* **82,** 053806 (2010).
34. Wang, Y-D. & Clerk, A. A. Using interference for high fidelity quantum state transfer in optomechanics. *Phys. Rev. Lett.* **108,** 153603 (2012).
35. Tian, L. Adiabatic state conversion and pulse transmission in optomechanical systems. *Phys. Rev. Lett.* **108,** 153604 (2012).
36. Barzanjeh, Sh., Abdi, M., Milburn, G. J., Tombesi, P. & Vitali, D. Reversible optical-to-microwave quantum interface. *Phys. Rev. Lett.* **109,** 130503 (2012).
37. McGee, S. A., Meiser, D., Regal, C. A., Lehnert, K. W. & Holland, M. J. Mechanical resonators for storage and transfer of electrical and optical quantum states. *Phys. Rev. A* **87,** 053818 (2013).
38. Thompson, J. D. *et al.* Strong dispersive coupling of a high-finesse cavity to a micromechanical membrane. *Nature* **452,** 72–75 (2008).
39. Purdy, T. P., Peterson, R. W. & Regal, C. A. Observation of radiation pressure shot noise on a macroscopic object. *Science* **339,** 801–804 (2013).
40. Yu, P-L., Purdy, T. P. & Regal, C. A. Control of material damping in high-*Q* membrane microresonators. *Phys. Rev. Lett.* **108,** 083603 (2012).
41. Bagci, T. *et al.* Optical detection of radio waves through a nanomechanical transducer. Preprint at http://arxiv.org/abs/1307.3467 (2013).
42. Akram, U., Kiesel, N. N., Aspelmeyer, M. & Milburn, G. J. Single-photon opto-mechanics in the strong coupling regime. *New J. Phys.* **12,** 083030 (2010).
43. Zhang, J., Peng, K. & Braunstein, S. L. Quantum-state transfer from light to macroscopic oscillators. *Phys. Rev. A* **68,** 013808 (2003).

44. Hill, J. T., Safavi-Naeini, A. H., Chan, J. & Painter, O. Coherent optical wavelength conversion via cavity optomechanics. *Nature Commun.* **3,** 1196 (2012).
45. Law, C. K. Interaction between a moving mirror and radiation pressure: A Hamiltonian formulation. *Phys. Rev. A* **51,** 2537–2541 (1995).
46. Caves, C. M. Quantum limits on noise in linear amplifiers. *Phys. Rev. D* **26,** 1817–1839 (1982).
47. Purdy, T. P., Peterson, R. W., Yu, P-L. & Regal, C. A. Cavity optomechanics with Si_3N_4 membranes at cryogenic temperatures. *New J. Phys.* **14,** 115021 (2012).
48. Wang, Y-D. & Clerk, A. A. Reservoir-engineered entanglement in optomechanical systems. *Phys. Rev. Lett.* **110,** 253601 (2013).
49. Tian, L. Robust photon entanglement via quantum interference in optomechanical interfaces. *Phys. Rev. Lett.* **110,** 233602 (2013).
50. Kuzyk, M. C., van Enk, S. J. & Wang, H. Generating robust optical entanglement in weak-coupling optomechanical systems. *Phys. Rev. A* **88,** 062341 (2013).
51. Zwickl, B. M. *et al.* High quality mechanical and optical properties of commercial silicon nitride membranes. *Appl. Phys. Lett.* **92,** 103125 (2008).

Acknowledgements

This work was supported by the DARPA QuASAR programme and the National Science Foundation under grant number 1125844. We would like to thank D. R. Schmidt for sharing his knowledge of fabrication techniques, J. N. Ullom for lending us equipment and P-L. Yu, J. D. Teufel and J. Kerckhoff for discussions. C.A.R. thanks the Clare Boothe Luce Foundation for support.

Author contributions

R.W.A. and R.W.P. made the measurements and analysed the data. R.W.A., R.W.P. and T.P.P. designed and constructed the experimental apparatus and optical device. R.W.A., K.C. and R.W.S. designed the electrical device. R.W.A. and K.C. fabricated the electrical device. C.A.R., R.W.S. and K.W.L. planned and supervised the experiment. R.W.A., R.W.P., C.A.R. and K.W.L. wrote the manuscript. All authors commented on the results and manuscript.

Additional information

Supplementary information is available in the online version of the paper. Reprints and permissions information is available online at www.nature.com/reprints. Correspondence and requests for materials should be addressed to R.W.A.

Competing financial interests

The authors declare no competing financial interests.